a

	CRAD		*APC*		*DCC*		*CTNNB1*		*AXIN2*		*HPRT1*	
Mutation	N	%	N	%	N	%	N	%	N	%	N	%
Substitution nonsense	5	3.18	1177	35.90	33	11.50	17	0.37	3	3.61	0	0
Substitution missense	97	61.78	494	15.07	207	72.13	3970	86.51	53	63.86	11	84.62
Substitution synonymous	38	24.20	171	5.22	60	20.91	90	1.96	13	15.66	3	23.08
Insertion inframe	11	7.01	3	0.09	0	0	6	0.13	0	0	0	0
Insertion frameshift	5	3.18	583	17.78	0	0	1	0.02	8	9.64	0	0
Deletion inframe	1	0.64	0	0	0	0	353	7.69	0	0	0	0
Deletion frameshift	6	3.82	1186	36.17	4	1.39	16	0.35	9	10.84	0	0
Nonsense + Frameshift (%)		10.18		89.85		12.09		0.74		24.09		0

b

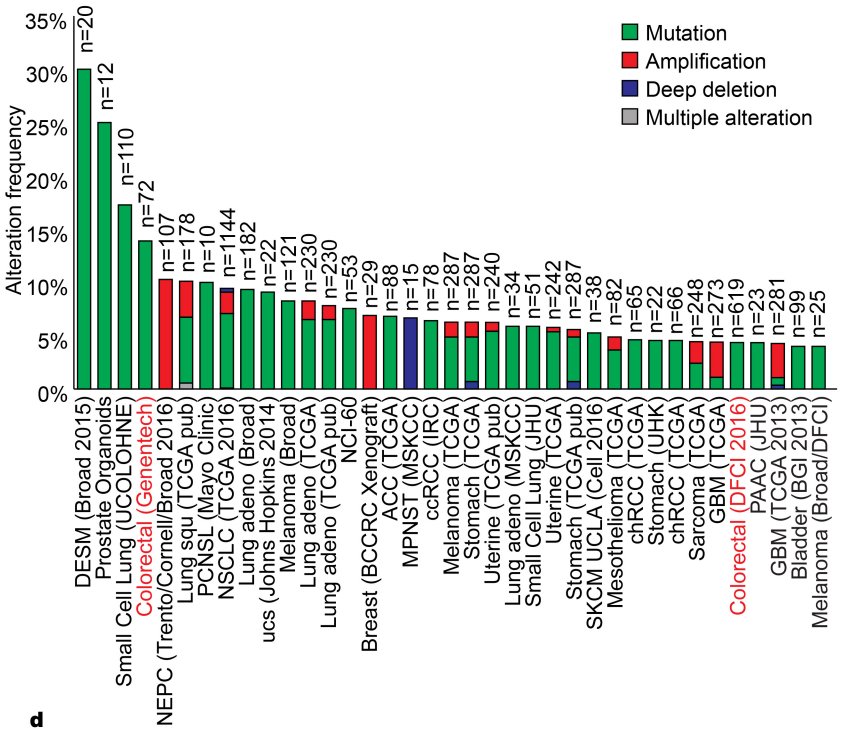

c

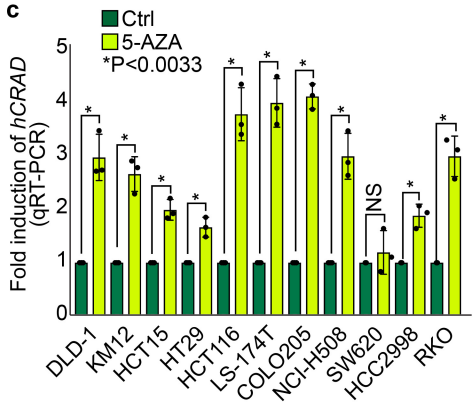

d

Cell line	Mutation	Cell line	Mutation	Cell line	Mutation
LIM2551	p.E309fs*115 (D)	LIM2405	p.Q324R (M)	RKO	p.A783T (M)
LIM2551	p.Q760fs*69 (D)	SW620	p.A501G (M)	HDC101	p.D15Y (M)
CCK81	p.K167fs*82 (D)	SW948	p.S975P (M)	SW48	p.A286V (M)
LIM1899	p.E309fs*115 (D)	HCT116	p.A511V (M)		

10 of 130 cell lines; M: Substitution-Missense; D: Deletion-Frame-shift

Supplementary Figure 1

Genetic inactivation of *CRAD* in cancer

a, Genetic inactivation of *CRAD* in CRC. cBioportal database analysis of *CRAD* in CRC. *CRAD* shows 10.18 % incidence rate of truncated mutants (Nonsense + Frameshift) in CRC. *APC*, *DCC*, *CTNNB1*, and *AXIN2* were analyzed as the positive control. *HPRP1* served as negative control. Total 502 CRC cases were analyzed.

b, Genetic alteration of *CRAD* in human cancer. cBioportal analysis.

c, Potent epigenetic suppression of CRAD promoter. Upregulated CRAD expression by the inhibition of methylation. IECs and CRC cells were treated with 5-Azacytidine (5-AZA; 20μM) for 24hr. n= 3 independent experiments; Error bars: average ± S.D.; NS: not significant (P>0.05); Two-sided unpaired *t*-test.

d, COSMIC analysis of *CRAD* mutations in CRC cell lines.

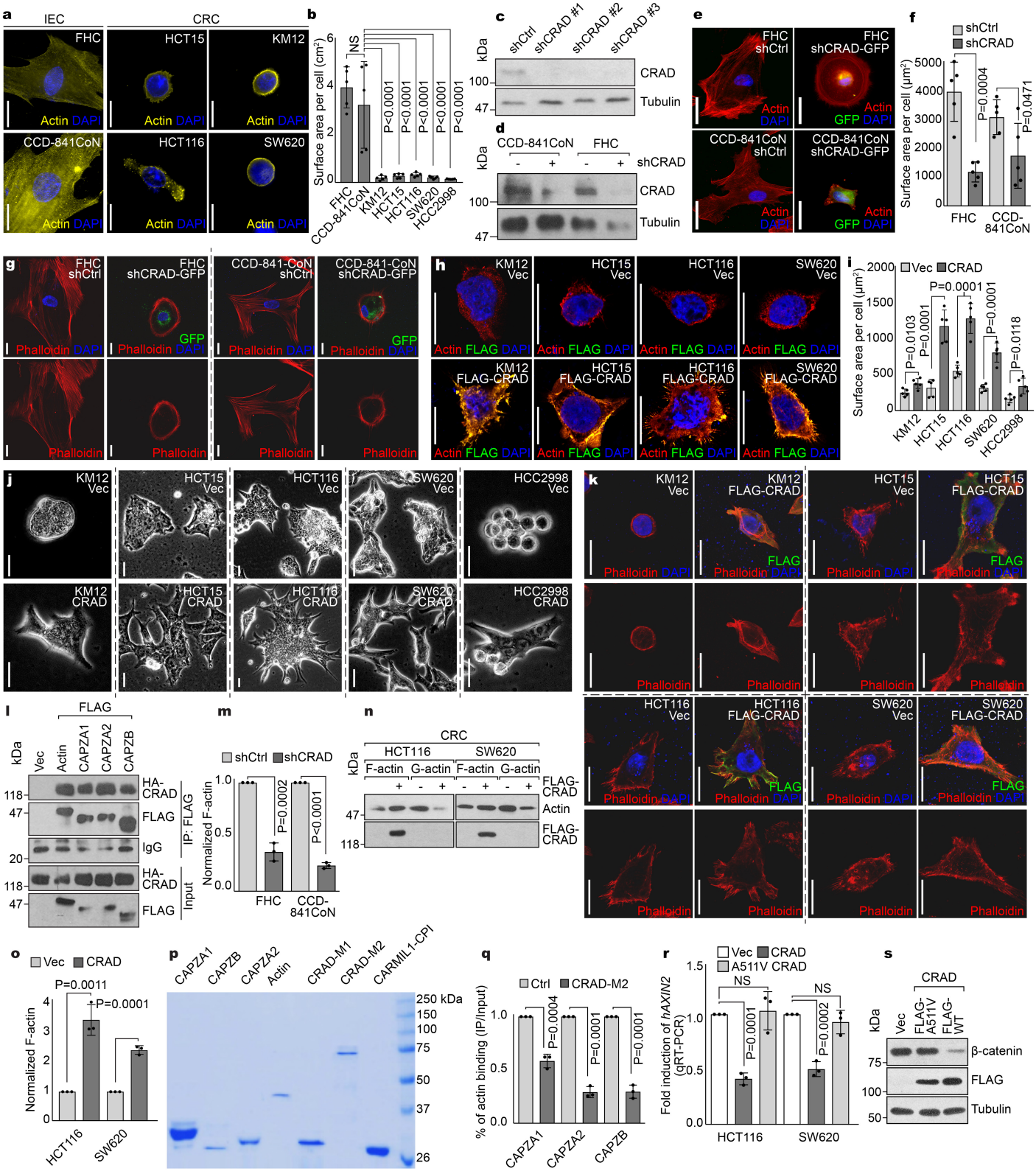

Supplementary Figure 2

Positive regulation of the actin polymerization by CRAD-induced capping protein inhibition

a and b, Morphological comparison of IECs and CRC cells. IF staining (**a**). Quantification of the cell area of IECs and CRC cells by AxioVision software (**b**; n= 5 independent experiments)

c and d, Depletion of endogenous CRAD by shRNAs. FHC cells were transfected with shRNAs (**c**). shCRAD#1 stably expressing IECs were analyzed for IB (**d**). IB was performed once.

e-g, Cell shrinkage by CRAD depletion. 48hr after transfection, cells were analyzed for IF staining (**e**) and cell area quantification (**f**; n=5 (independent experiments). Cells were infected with lenti-shCRAD for 48hr. After infection, cells were selected by puromycin (2μg/ml) treatment for 72hr. The cell morphology was analyzed by IF staining for Phalloidin (**g**).

h-k, Extended cell morphology by CRAD in CRC cells. 48hr after transfection (Vec [empty vector] or FLAG-CRAD), cells were analyzed for IF staining (actin, **h**; Phalloidin, **k**) and cell area quantification (**i**; n=5 independent experiments). The cell morphology was monitored using blight field microscope (**j**).

l, Physical interaction of CRAD with CPs. Purified FLAG-Actin, FLAG-CPs, and HA-CRAD proteins were used for co-IP. These results recapitulate *in vitro* interaction between CRAD and CPs performed using GST recombinant proteins. Experiment was performed three times with similar results.

m-o, Decreased F-actin formation by *CRAD* depletion. Quantification of the F-actin in the *CRAD* depleted (**m**), or the *CRAD* ectopic expressed condition (**n and o**). The level of F-actin and G-actin was examined by immunoblots (**n**) and quantified by the subsequent ImageJ analysis (**m and o**; n=3 independent experiments). After measurement, F-actin was normalized by G-actin.

p, Coomassie Brilliant Blue (CBB) staining of the purified recombinant proteins. Each recombinant protein was expressed in *E. coli* and purified, followed by GST cleavage. Experiment was performed once.

q, Inhibition of interaction between CAPZs and actin by CRAD. Co-IP assay using purified recombinant proteins (see Fig. 2m) was quantified by ImageJ. n=3 independent experiments)

r and s. No effect of A511V-CRAD on Wnt/β-catenin signaling. *AXIN2* qRT-PCR (**r**; n=independent experiments) and IB (**s**) using WT-CRAD or A511V-CRAD transfected CRC cells. IB was performed three times with similar results.

Representative images are shown; Scale bars indicate 20μm; Error bars: mean ± S.D.; NS: not significant (P>0.05); Two-sided unpaired *t*-test.

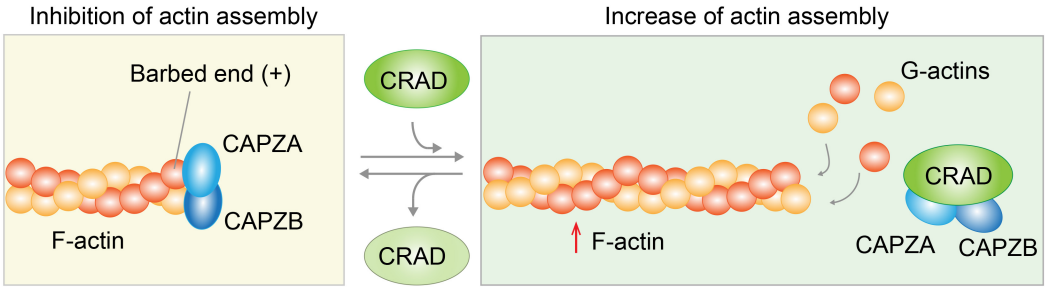

Supplementary Figure 3

Illustration of the working model of CRAD-induced F-actin polymerization.

CRAD inhibits CPs' binding to the barbed (+) end, resulting in the increased actin polymerization.

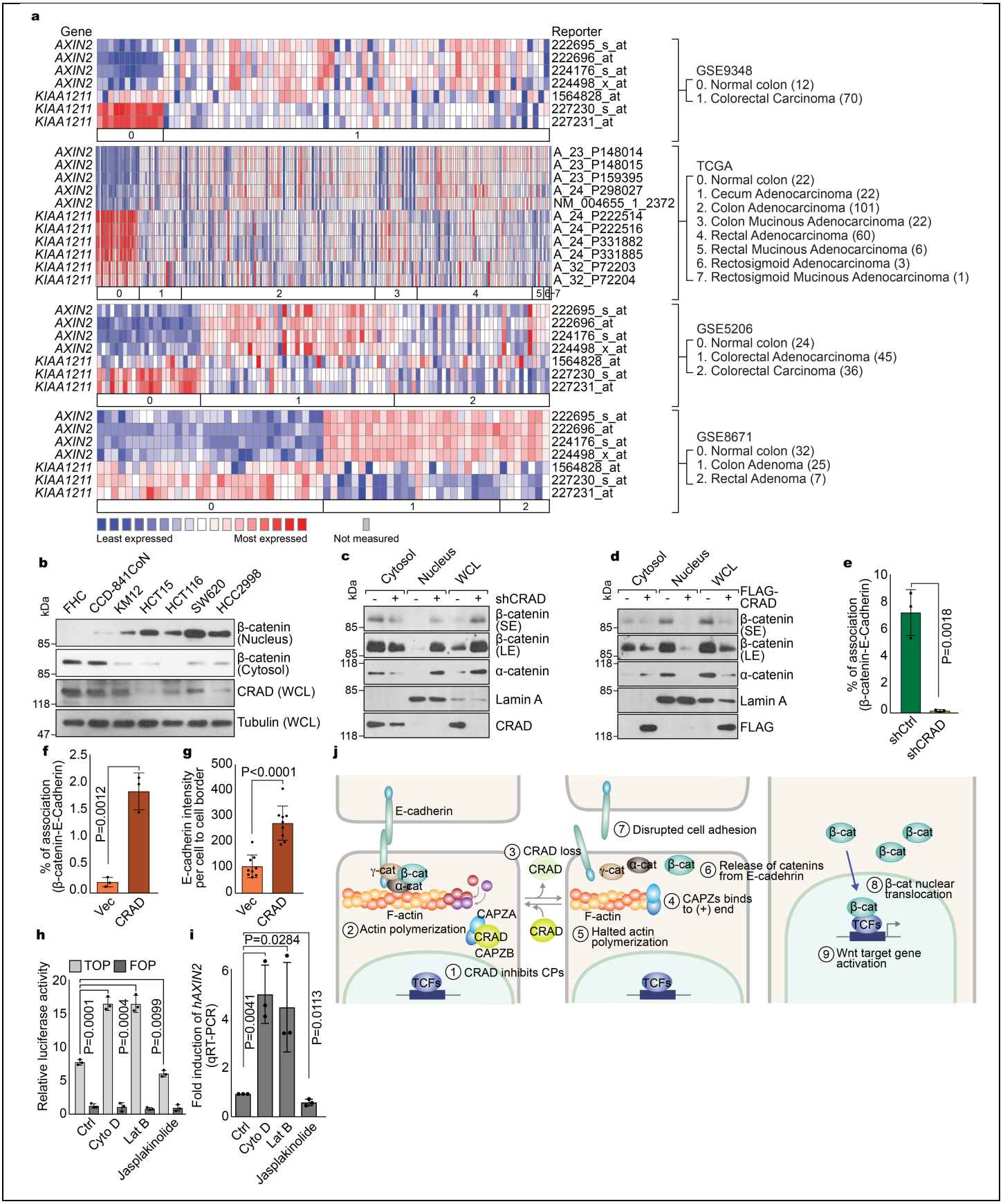
a
Gene
Reporter
AXIN2
KIAA1211
222695_s_at
222696_at
224176_s_at
224498_x_at
1564828_at
227230_s_at
227231_at
GSE9348
0. Normal colon (12)
1. Colorectal Carcinoma (70)
A_23_P148014
A_23_P148015
A_23_P159395
A_24_P298027
NM_004655_1_2372
A_24_P222514
A_24_P222516
A_24_P331882
A_24_P331885
A_32_P72203
A_32_P72204
TCGA
0. Normal colon (22)
1. Cecum Adenocarcinoma (22)
2. Colon Adenocarcinoma (101)
3. Colon Mucinous Adenocarcinoma (22)
4. Rectal Adenocarcinoma (60)
5. Rectal Mucinous Adenocarcinoma (6)
6. Rectosigmoid Adenocarcinoma (3)
7. Rectosigmoid Mucinous Adenocarcinoma (1)
GSE5206
0. Normal colon (24)
1. Colorectal Adenocarcinoma (45)
2. Colorectal Carcinoma (36)
GSE8671
0. Normal colon (32)
1. Colon Adenoma (25)
2. Rectal Adenoma (7)
Least expressed
Most expressed
Not measured
b
kDa
FHC
CCD-841CoN
KM12
HCT15
HCT116
SW620
HCC2998
β-catenin (Nucleus)
β-catenin (Cytosol)
CRAD (WCL)
Tubulin (WCL)
c
Cytosol
Nucleus
WCL
shCRAD
β-catenin (SE)
β-catenin (LE)
α-catenin
Lamin A
CRAD
d
FLAG-CRAD
FLAG
e
% of association (β-catenin-E-Cadherin)
P=0.0018
shCtrl
shCRAD
f
P=0.0012
Vec
CRAD
g
E-cadherin intensity per cell to cell border
P<0.0001
h
TOP
FOP
Relative luciferase activity
P=0.0001
P=0.0004
P=0.0099
Ctrl
Cyto D
Lat B
Jasplakinolide
i
Fold induction of hAXIN2 (qRT-PCR)
P=0.0284
P=0.0041
P=0.0113
j
E-cadherin
γ-cat
β-cat
α-cat
F-actin
CAPZA
CRAD
CAPZB
TCFs
① CRAD inhibits CPs
② Actin polymerization
③ CRAD loss
④ CAPZs binds to (+) end
⑤ Halted actin polymerization
⑥ Release of catenins from E-cadehrin
⑦ Disrupted cell adhesion
⑧ β-cat nuclear translocation
⑨ Wnt target gene activation

Supplementary Figure 4

CRC cell growth inhibition by CRAD

a, The mutually exclusive expression between *CRAD* and *AXIN2* in IECs and CRC. Oncomine analysis of *CRAD* and *AXIN2* expression in CRC.

b, Inversed correlation between CRAD and β-catenin. IECs and CRC cells were fractionated into the nucleus and cytosol fractions using fractionation kit. WCL: whole cell lysates.

c and d, Decreased nuclear β-catenin by CRAD. IECs (**c**) and CRC cells (**d**) were transfected with shCtrl or shCRAD and Vec or CRAD, respectively. After 48hr, cells were fractionated into the cytosolic and nucleus fractions, followed by IB.

e and f, Increased interaction between E-Cadherin and β-catenin by CRAD. Cell extracts from IEC (**e**) and CRC cell (**f**) were used for IP analysis. Binding between E-Cadherin and β-catenin was quantified by ImageJ. n=3.

g, Increased interaction between E-cadherin and catenins by CRAD. HCT116 cells were transiently transfected with FLAG-CRAD plasmid and analyzed for IF staining using Super Resolution microscope (see Fig. 3p). E-cadherin intensity was quantified by ZEN software (Zeiss). n=10.

h and i, Blockade of the actin cytoskeleton increases Wnt/β-catenin reporter activity. CCD-841CoN cells were transfected with β-catenin reporter plasmids (pMEGA-TOP/FOP-FLASH). 24hr after, cells were treated with Cytochalasin D (Cyto D; 2μM; barbed [+] end inhibition)[51], Latrunculin B (Lat B; 1μM; monomeric G-actin inhibition)[52], and Jasplakinolide (2μM; a stabilizer of actin cytoskeleton) for 72hr. β-catenin transcription activity was measured by TOP/FOP luciferase activity (**h**). CCD-841CoN cells were treated with indicated reagents as same concentration of (**h**). 72hr after treatment, cells were collected for qRT-PCR (**i**). n=3 independent experiments.

j, Illustration of the working model: the molecular mechanism of CRAD loss-induced hyperactivation of Wnt/β-catenin signaling. In normal epithelial cells, CRAD inhibits CPs, which results in actin polymerization. Subsequently, increased F-actin stabilizes complex formation composed of E-cadherin-catenins-F-actin. In the absence of CRAD, F-actin is disrupted by CPs, which leads to destabilization of E-cadherin-catenin complex. Disturbance of E-cadherin-catenin complex releases β-catenin into the cytosols and the nucleus, which transactivates Wnt/β-catenin target genes.

Error bars: average ± S.D.; Two-sided unpaired *t*-test; Centre: Average.

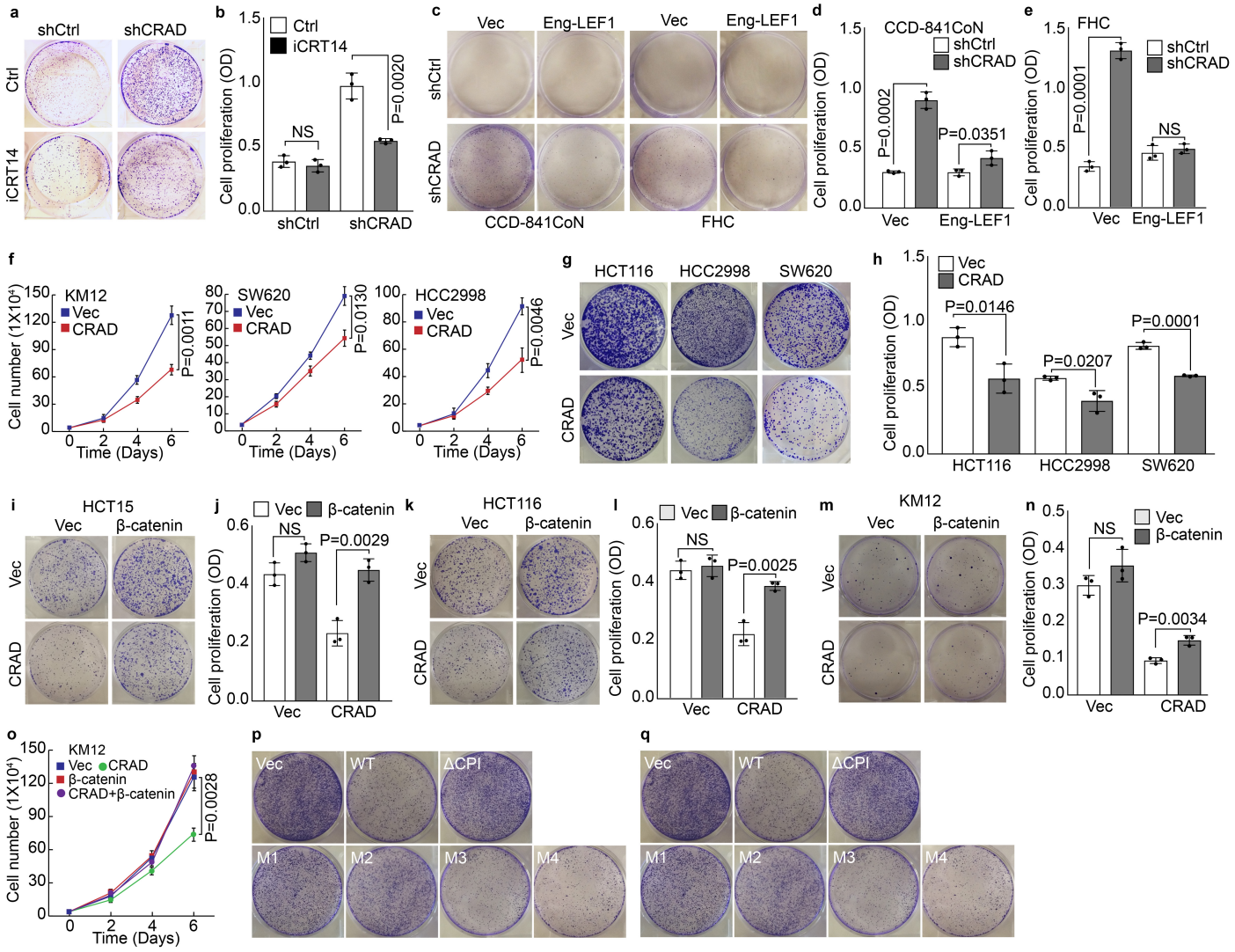

Supplementary Figure 5

CRC cell growth inhibition by CRAD

a and b, Suppression of shCRAD-induced cell hyperproliferation by β-catenin inhibition in IECs. FHC (shCtrl and shCRAD) cells were treated with iCRT14 for 14 days and stained with crystal violet (**a**). Cell proliferation was quantified by measurement of absorbance at 590nm (**b**; n=3 independent experiments).

c-e, Engrailed-LEF1 inhibits *CRAD* depletion-induced IEC hyperproliferation. 1,000 cells of CCD-841CoN were seeded onto tissue culture plate. Cells were transfected with indicated plasmids. Eng-LEF1 was used as a dominant-negative mutant blocker of β-catenin-mediated gene transactivation[53, 54]. 48hr after transfection, cells were incubated in 37°C tissue culture CO_2 chamber for 14 days. Colony forming was visualized by crystal violet staining (**c**) and quantified (**d and e**; n=3 independent experiments).

f-h, CRC cell growth inhibition by CRAD expression. CRC cells (Vec [control] and CRAD expressing) were analyzed for cell counting (**f**; n=3 independent experiments), crystal violet staining (**g**), and quantification (**h**).

i-o, β-catenin rescues CRAD-induced CRC cell growth inhibition. CRC cells were transfected with CRAD or-catenin plasmids and analyzed for crystal violet staining (**i,k,m**), quantification (**j, l, n**), and cell counting (**o**).

p and q, CRC cell growth inhibition by CPI motif-containing CRAD mutants. CRAD (FL, ΔCPI, and M1-M4)-transfected CRC cells were analyzed for quantification of cell proliferation. HCT116 (**p**); SW620 cells (**q**).

Representative images are shown; Error bars: mean ± S.D.; NS: not significant (P>0.05); Two-sided unpaired *t*-test.

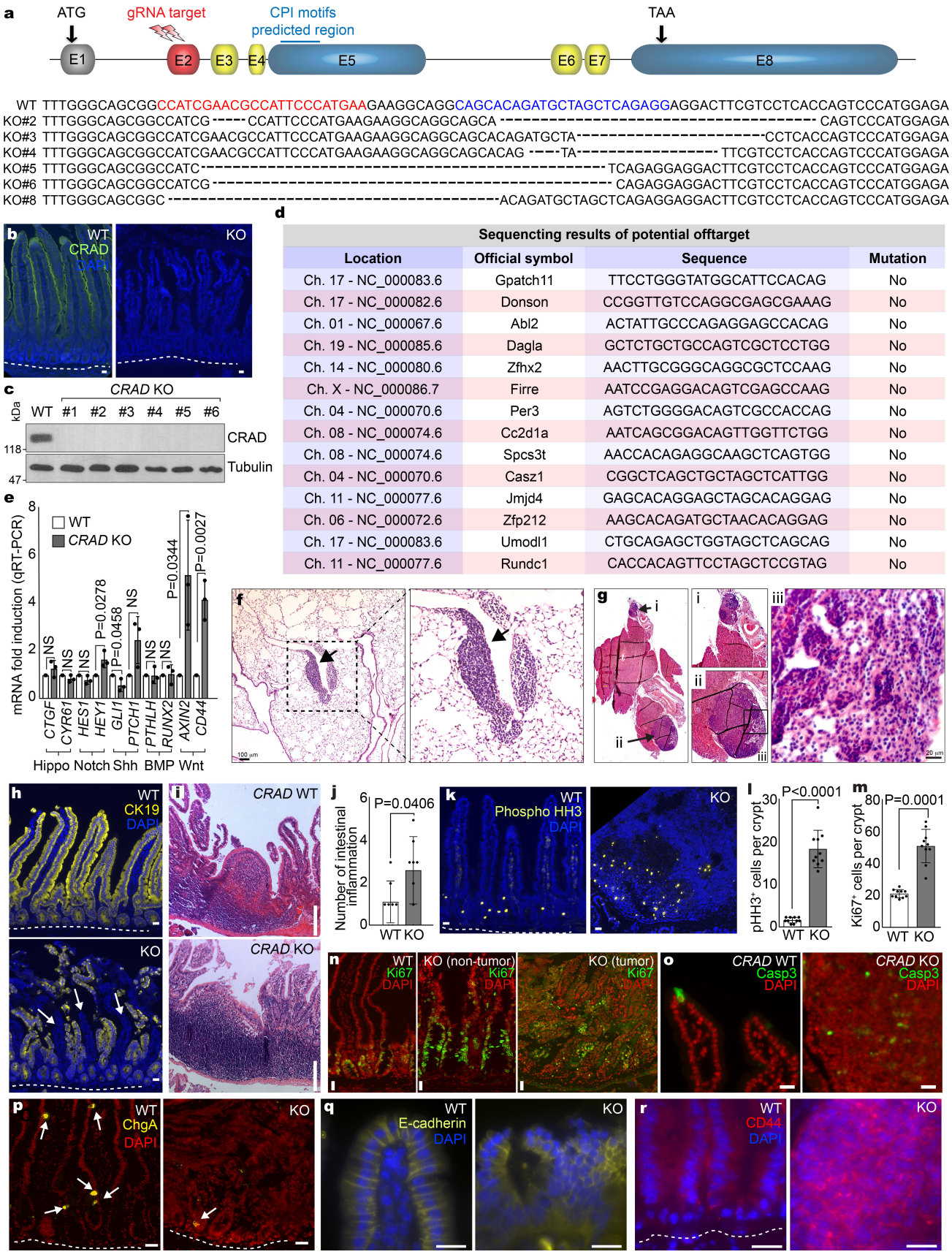

Sequencting results of potential offtarget			
Location	**Official symbol**	**Sequence**	**Mutation**
Ch. 17 - NC_000083.6	Gpatch11	TTCCTGGGTATGGCATTCCACAG	No
Ch. 17 - NC_000082.6	Donson	CCGGTTGTCCAGGCGAGCGAAAG	No
Ch. 01 - NC_000067.6	Abl2	ACTATTGCCCAGAGGAGCCACAG	No
Ch. 19 - NC_000085.6	Dagla	GCTCTGCTGCCAGTCGCTCCTGG	No
Ch. 14 - NC_000080.6	Zfhx2	AACTTGCGGGCAGGCGCTCCAAG	No
Ch. X - NC_000086.7	Firre	AATCCGAGGACAGTCGAGCCAAG	No
Ch. 04 - NC_000070.6	Per3	AGTCTGGGGACAGTCGCCACCAG	No
Ch. 08 - NC_000074.6	Cc2d1a	AATCAGCGGACAGTTGGTTCTGG	No
Ch. 08 - NC_000074.6	Spcs3t	AACCACAGAGGCAAGCTCAGTGG	No
Ch. 04 - NC_000070.6	Casz1	CGGCTCAGCTGCTAGCTCATTGG	No
Ch. 11 - NC_000077.6	Jmjd4	GAGCACAGGAGCTAGCACAGGAG	No
Ch. 06 - NC_000072.6	Zfp212	AAGCACAGATGCTAACACAGGAG	No
Ch. 17 - NC_000083.6	Umodl1	CTGCAGAGCTGGTAGCTCAGCAG	No
Ch. 11 - NC_000077.6	Rundc1	CACCACAGTTCCTAGCTCCGTAG	No

Supplementary Figure 6

Intestinal adenoma development by *CRAD* KO

a, CRISPR/Cas9-mediated targeting of *CRAD* alleles. Exon2 of *CRAD* was targeted using gRNAs. gRNA and Cas9 mRNA were injected into the pronuclei of C57BL/B6 mouse embryos.

b, CRAD expression in the small intestine. IHC of mouse intestine.

c, Validation of *CRAD* KO. The cell lysates were extracted from the small intestine of six independent *CRAD* KO mice for IB.

d, Sequencing analysis of potential off-target genes of *CRAD* gRNAs. No mutations in 14 off-target genes were detected.

e, Increased Wnt signaling target genes in *CRAD* KO mouse. *CRAD* KO-induced tumors were analyzed for qRT-PCR of Hippo, Notch, Shh, BMP, and Wnt signaling pathway target genes. n=3 independent mice.

f and g, Tumor development in the lung and pancreas of *CRAD* KO mice. Development of the early lesion of SCLC. The multiple sites displaying the early lesion of SCLC (black arrows; **f**) and the pancreatic tumors (**g**; i and ii) were observed. Scale bars indicate 100μm (**f**) or 20μm (**g**).

h, Disruption of epithelial cell integrity. Cytokeratin 19 (CK19). Arrows: Villi not expressing CK19.

i and j, Analysis of inflammation in *CRAD* KO mouse. Small intestine samples of WT and *CRAD* KO mouse were stained with H&E (**i**; n=8 mice). Intestinal inflammation (*foci* size > 200μm) was assessed by counting (**j**). Scale bars indicate 200μm.

k-n, Cell hyperproliferation in *CRAD* KO small intestine. Phospho-histone H3 (**k**) and Ki67 (**n**) staining and quantification (**l and m**; n=10 crypts). Scale bars indicate 20μm.

o, Analysis of apoptosis in *CRAD* KO-induced tumor lesion. WT and *CRAD* KO mice were analyzed for cleaved Caspase-3 (Casp3). Scale bars indicate 20μm.

p, Abnormal differentiation of IECs by *CRAD* KO. WT and *CRAD* KO small intestine were immunostained with ChgA (arrows). Scale bars indicate 20μm.

q, Disorganized cell adhesion in *CRAD* KO mice. Cells were stained with E-cadherin. Scale bars indicate 20μm.

r, Increased β-catenin target genes in the intestinal adenoma of *CRAD* KO mice. IHC for CD44. Scale bars indicate 20μm.

Representative images of three independent experiments; Error bars: mean ± S.D.; NS: not significant (P>0.05); Two-sided unpaired *t*-test.

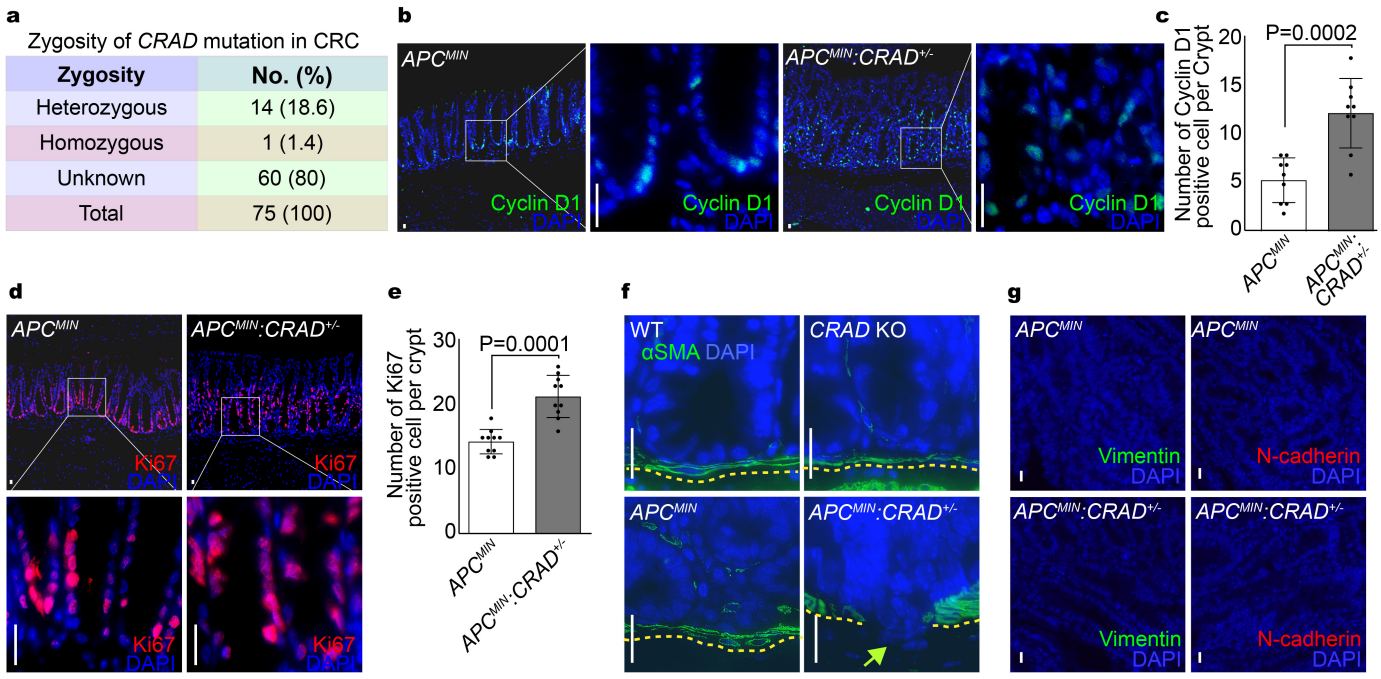

Supplementary Figure 7

Accelerated intestinal tumorigenesis by *CRAD* heterogeneous KO

a, Heterozygous mutation of *CRAD* gene in CRC. Zygosity analysis of *CRAD* mutation in CRC patient samples using COSMIC and cBioportal databases. Of note, the frequency of heterozygous mutation is higher than that of homozygous mutation.

b-e, IHC of the non-tumor region of the colorectum of APC^{MIN} and APC^{MIN}:$CRAD^{+/-}$ mice (4mo of age). Cyclin D1 (**b**); Ki67 (**d**). Quantification (**c;** n=9 crypts**, e**; n=10 crypts).

f, Micro-invasion by *CRAD* KO. Micro-invasion was observed in the tumor region of APC^{MIN}:$CRAD^{+/-}$ small intestine. The small intestine samples were stained with αSMA (α-Smooth Muscle Actin: green) to visualize the basement membrane. The basement membrane of APC^{MIN}:$CRAD^{+/-}$ is disrupted/discontinued tumor cell infiltration. Arrow indicates invasive tumor cell and yellow dashed lines mark the border of the basement membrane.

g, No EMT in tumor region of APC^{MIN}:$CRAD^{+/-}$ mice. EMT marker analysis in APC^{MIN} and APC^{MIN}:$CRAD^{+/-}$ small intestine samples. Markers of mesenchymal cell (Vimentin: green; N-cadherin: red) were not detected in tumors of both strains.

Representative images of three independent experiments; Scale bars indicate 20μm; Error bars: mean ± S.D.; Two-sided unpaired *t*-test.

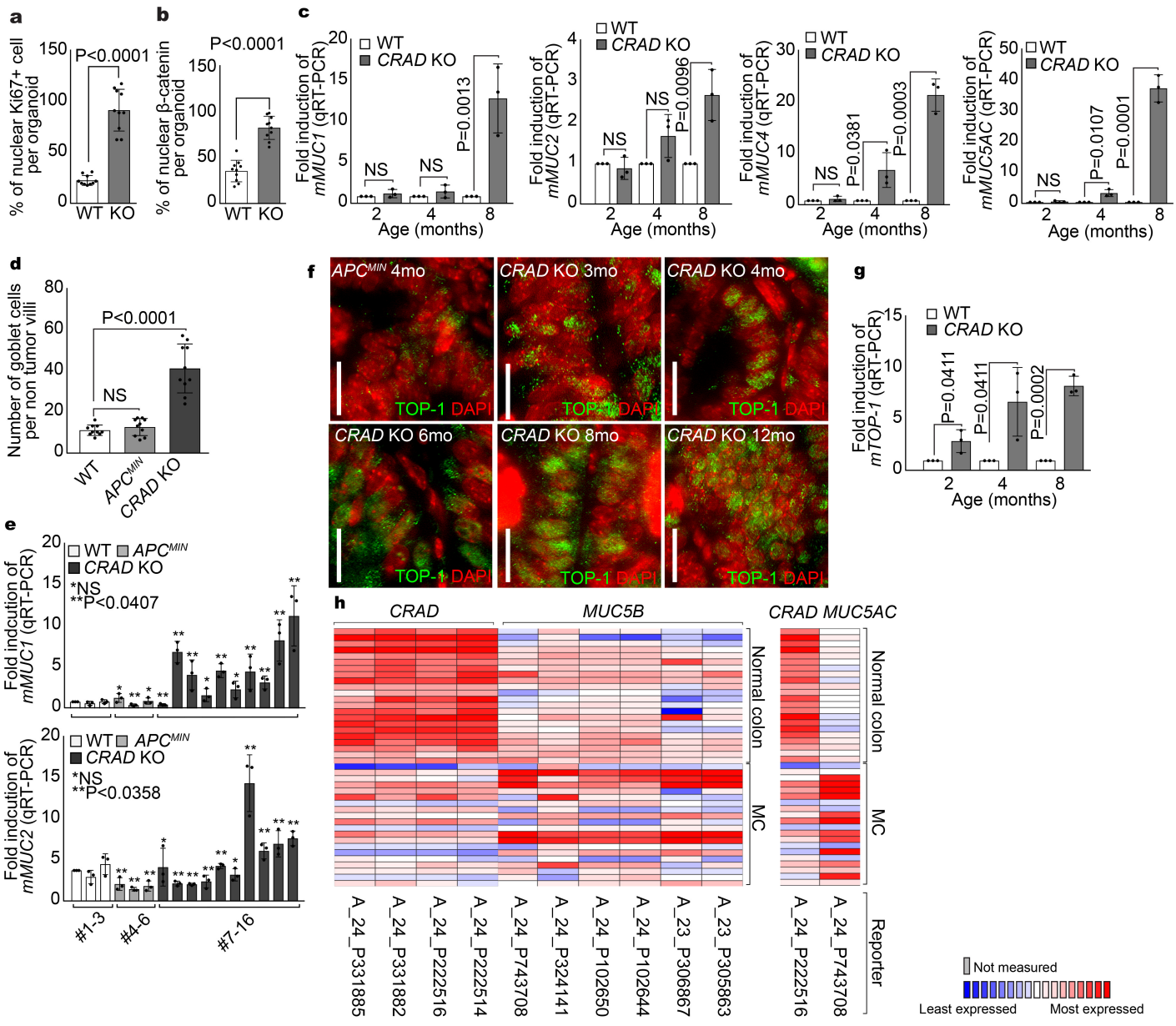

Supplementary Figure 8

Accelerated intestinal tumorigenesis by *CRAD* KO

a and b, IHC analysis of the organoids derived from *CRAD* WT and KO mouse intestine. Compared to WT, *CRAD* KO-derived cystic spheroids showed the increased cell proliferation (Ki67; **a**) and the increase of β-catenin (**b**). Quantification was performed using 10 cystic spheroids. n=10 organoids from three different experiments.

c, Increased *Mucin* expression in *CRAD* KO. The small intestine samples from *CRAD* WT (2mo) and *CRAD* KO mice (from different ages as indicated) were examined by qRT-PCR for *mMUC1, mMUC2, mMUC4,* and *mMUC5AC*. n=3 independent experiments.

d, Increased goblet cell in *CRAD* KO mice. After fixation and paraffin embedding, each sample was stained with PAS and quantified. n=10 villi.

e, Increased mucin deposition in *CRAD* KO-induced tumors. qRT-PCR of *MUC1* and *MUC2* from the small intestine samples of each mice. n=3 independent experiments.

f, The increase of TOP-1 expression in *CRAD* KO mouse. Tumor of APC^{MIN} (4mo) and *CRAD* KO (3, 4, 6, 8, and 12mo) were immunostained with a TOP-1 antibody.

g, Upregulation of *TOP-1* in *CRAD* KO tumors. *CRAD* WT (2mo) intestine and *CRAD* KO tumors (from different age were examined by qRT-PCR of mTOP-1. n=3 independent experiments.

h, Mutual exclusive expression of *CRAD* and *MUCs*. Oncomine analysis of TCGA datasets; 10% gene rank; $P<0.0001$; fold change >2; compared with normal cells.

Representative images of three independent experiments; Scale bars indicate 20μm; Error bars: mean ± S.D.; NS: not significant ($P>0.05$); Two-sided unpaired *t*-test.

SCANNED WB #1

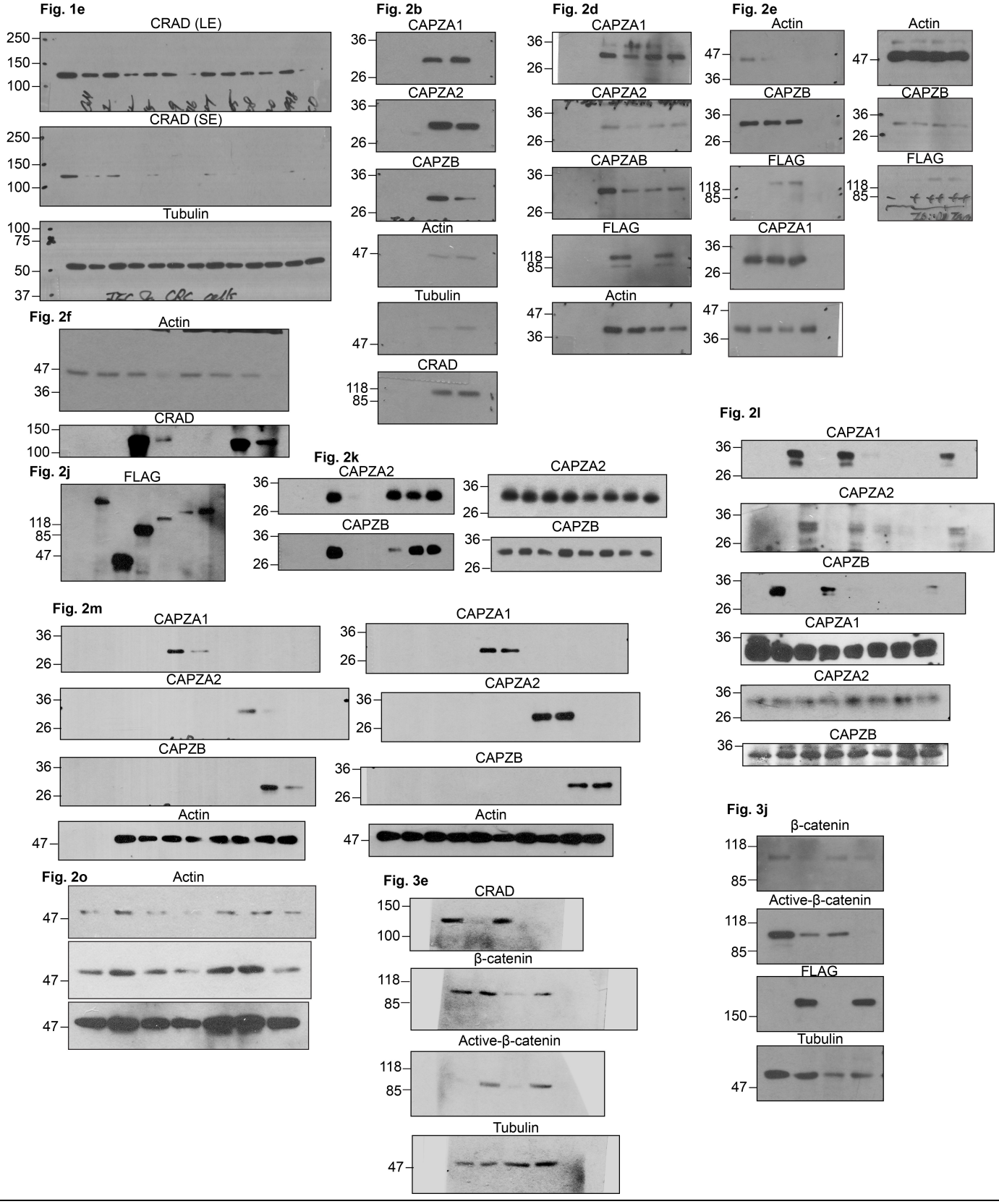
Fig. 1e
CRAD (LE)
250
150
100
CRAD (SE)
250
150
100
Tubulin
100
75
50
37
Fig. 2b
CAPZA1
36
26
CAPZA2
36
26
CAPZB
36
26
Actin
47
Tubulin
47
CRAD
118
85
Fig. 2d
CAPZA1
36
26
CAPZA2
36
26
CAPZAB
36
26
FLAG
118
85
Actin
47
36
Fig. 2e
Actin
47
36
CAPZB
36
26
FLAG
118
85
CAPZA1
36
26
Actin
47
CAPZB
36
26
FLAG
118
85
Fig. 2f
Actin
47
36
CRAD
150
100
Fig. 2j
FLAG
118
85
47
Fig. 2k
CAPZA2
36
26
CAPZB
36
26
CAPZA2
36
26
CAPZB
36
26
Fig. 2l
CAPZA1
36
26
CAPZA2
36
26
CAPZB
36
26
CAPZA1
36
CAPZA2
36
26
CAPZB
36
Fig. 2m
CAPZA1
36
26
CAPZA2
36
26
CAPZB
36
26
Actin
47
CAPZA1
36
26
CAPZA2
36
26
CAPZB
36
26
Actin
47
Fig. 2o
Actin
47
47
47
Fig. 3e
CRAD
150
100
β-catenin
118
85
Active-β-catenin
118
85
Tubulin
47
Fig. 3j
β-catenin
118
85
Active-β-catenin
118
85
FLAG
150
Tubulin
47

Supplementary Figure 9
Unprocessed blots
Figs. 1e-3j

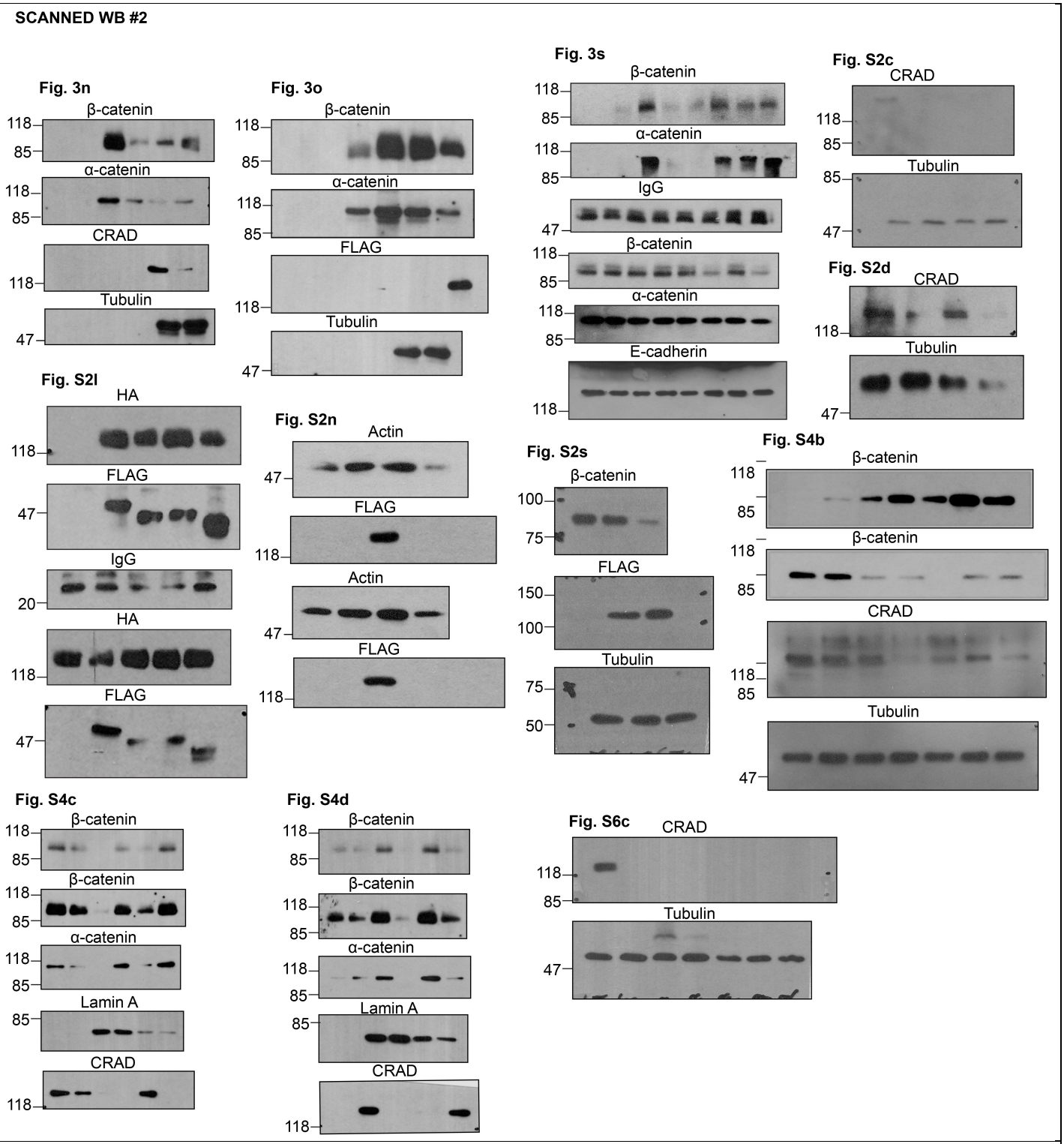

Supplementary Figure 10

Unprocessed blots

Figs. 3n-S6c

Supplementary Table 1 Analysis of CRC tumor microarray for CRAD expression.

To determine CRAD protein expression, we analyzed 38 colon adenocarcinoma samples, 2 signet-ring cell carcinoma, and 14 normal colonic tissue samples using IHC for CRAD. While CRC samples show the low or absence of CRAD expression (colon adenocarcinoma: 12/44 [27%]; signet-ring cell carcinoma: 0/2 [0%]), normal tissue samples display the high expression of CRAD protein (14/14; 100%). NA: not applicable (due to the sample quality, these samples were excluded from analysis; 1: high expression; 0.5: low expression; 0: not detected).

Supplementary Table 2 CRAD-interacting proteins identified by tandem affinity purification and mass spectrometry.

293T cells stably expressing CRAD tagged with protein S, FLAG, Streptavidin-binding peptide (SFB) were processed for tandem affinity purification and mass spectrometry (TAP-MS/MS). Total 362 proteins were identified as CRAD-binding proteins. The number of peptides and peptide coverage are also included.

Supplementary Table 3 Information of MC microarray for CRAD expression.

To determine CRAD protein expression, we analyzed 34 MC and normal colonic tissue samples (Biomax; OD-CT-DgCol03-003 : Colon mucinous adenocarcinoma tissue array) using IHC for CRAD. While MC samples show the low or absence of CRAD expression normal tissue samples display the high expression of CRAD protein. TNM grading: T - Primary tumor; N - Regional lymph nodes; M - Distant metastasis.

Supplementary Table 4 Primer information.

A complete list of primers.

Supplementary Table 5 Antibody information.

A complete list of antibodies.

Supplementary Table 6 Statistics Source Data.

14 sheets contain statistics source data.

References

51. MacLean-Fletcher, S. & Pollard, T.D. Mechanism of action of cytochalasin B on actin. *Cell* **20**, 329-341 (1980).

52. Morton, W.M., Ayscough, K.R. & McLaughlin, P.J. Latrunculin alters the actin-monomer subunit interface to prevent polymerization. *Nat Cell Biol* **2**, 376-378 (2000).

53. Hirsch, F.R. *et al.* Epidermal growth factor receptor in non-small-cell lung carcinomas: correlation between gene copy number and protein expression and impact on prognosis. *J Clin Oncol* **21**, 3798-3807 (2003).

54. John, T., Liu, G. & Tsao, M.S. Overview of molecular testing in non-small-cell lung cancer: mutational analysis, gene copy number, protein expression and other biomarkers of EGFR for the prediction of response to tyrosine kinase inhibitors. *Oncogene* **28 Suppl 1**, S14-23 (2009).